Inorg. Chem. **2005**, *44*, 7559–7569

Phosphate Triester Hydrolysis Promoted by an N_2S(thiolate)Zn Complex: Mechanistic Implications for the Metal-Dependent Reactivity of Peptide Deformylase

David P. Goldberg,*,† Robert C. diTargiani,† Frances Namuswe,† Ellen C. Minnihan,† SeChin Chang,† Lev N. Zakharov,‡ and Arnold L. Rheingold‡

Department of Chemistry, Johns Hopkins University, 3400 North Charles Street, Baltimore, Maryland 21218, and Department of Chemistry and Biochemistry, University of California, San Diego, 9500 Gilman Drive, La Jolla, California 92093

Received July 11, 2005

The zinc(II) complex (PATH)ZnOH, where PATH is an N_2S(thiolate) ligand, has been investigated for its ability to promote the hydrolysis of the phosphate triester tris(4-nitrophenyl) phosphate (TNP). The hydrolysis of TNP was examined as a function of PATH–zinc(II) complex concentration, substrate concentration, and pH in a water/ethanol mixture (66:33 v/v) at 25 °C. The reaction is first order in both zinc(II) complex and substrate, and the second-order rate constants were derived from linear plots of the observed pseudo-first-order rate constants versus zinc complex concentration at different pH values. A pH–rate profile yielded a kinetic pK_a of 8.52(5) for the zinc-bound water molecule and a pH-independent rate constant of 16.1(7) M^{-1} s^{-1}. Temperature-dependent studies showed linear Eyring behavior, yielding the activation parameters $\Delta H^{\ddagger} = 36.9(1)$ kJ mol^{-1} and $\Delta S^{\ddagger} = -106.7(4)$ J mol^{-1} K^{-1}. Interpretation of the kinetic data leads to the conclusion that hydrolysis of TNP takes place through a hybrid mechanism, in which the metal center plays a dual role of providing a nucleophilic hydroxide and activating the substrate through a Lewis acid effect. The synthesis and structural characterization of the related nickel(II) and iron(II) complexes $[(PATH)_2Ni_2]Br_2$ (**2**) and $(PATH)_2Fe_2Cl_2$ (**3**) are also described. Taken together, these data suggest a possible explanation for the low reactivity of the zinc(II) form of peptide deformylase as compared to the iron(II) form.

Introduction

Zinc enzymes comprise a large class of metalloproteins that have been extensively studied.[1−3] A subset of this class is the mononuclear zinc enzymes, which typically contain a pseudotetrahedral zinc ion bound to the protein through a combination of three His, Asp, Glu, or Cys residues. These enzymes catalyze the hydrolysis or hydration of a substrate via a coordinated H_2O/OH^- molecule, and their amidase/peptidase activity is of particular importance. A short sequence motif, HEXXH, is often conserved in these proteins with two of the His ligands coordinated to the zinc ion. One metallohydrolase that seemingly belongs to this family is peptide deformylase (PDF), which contains the HEXXH motif and has been structurally characterized with different divalent metal ions (Zn, Co, Ni, and Fe) coordinated in a two 2-His/1-Cys/1-$H_2O(OH^-)$ tetrahedral environment in the active site.[4−8] Previously, the zinc(II) form of PDF (Zn−PDF) had been ruled out as the active form in vivo, and instead the iron(II) enzyme (Fe(II)−PDF) was accepted as the native form.[4,6,9] However, recent work has pointed to at least one highly active Zn−PDF in plants (PDF1A).[10]

PDF catalyzes the hydrolysis of a formyl group according to eq 1. Examination of the metal dependence of the reactivity of PDF isolated from bacteria has shown that Zn−

* To whom correspondence should be addressed. E-mail: dpg@jhu.edu.
† Johns Hopkins University.
‡ University of California.

(1) Parkin, G. *Chem. Rev.* **2004**, *104*, 699−767.
(2) Lipscomb, W. N.; Sträter, N. *Chem. Rev.* **1996**, *96*, 2375−2433.
(3) Vallee, B. L.; Auld, D. S. *Acc. Chem. Res.* **1993**, *26*, 543−551.
(4) Baldwin, E. T.; Harris, M. S.; Yem, A. W.; Wolfe, C. L.; Vosters, A. F.; Curry, K. A.; Murray, R. W.; Bock, J. H.; Marshall, V. P.; Cialdella, J. I.; Merchant, M. H.; Choi, G.; Deibel, M. R., Jr. *J. Biol. Chem.* **2002**, *277*, 31163−31171.
(5) Hao, B.; Gong, W.; Rajagopalan, P. T. R.; Zhou, Y.; Pei, D.; Chan, M. K. *Biochemistry* **1999**, *38*, 4712−4719.
(6) Becker, A.; Schlichting, I.; Kabsch, W.; Groche, D.; Schultz, S.; Wagner, A. F. V. *Nat. Struct. Biol.* **1998**, *5*, 1053−1058.
(7) Becker, A.; Schlichting, I.; Kabsch, W.; Schultz, S.; Wagner, A. F. V. *J. Biol. Chem.* **1998**, *273*, 11413−11416.
(8) Chan, M. K.; Gong, W.; Rajagopalan, P. T. R.; Hao, B.; Tsai, C. M.; Pei, D. *Biochemistry* **1997**, *36*, 13904−13909.

10.1021/ic0511571 CCC: $30.25
Published on Web 09/16/2005

PDF is the least reactive compared to Fe(II)−, Ni(II)−, or Co(II)−PDF,[9,11,12] except in the case of a PDF isolated from *Leptospira interrogans*, which appears to resemble PDF1A.[13]

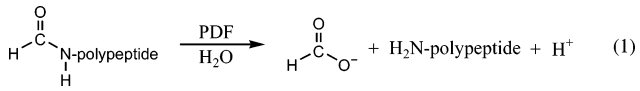

(1)

Given Nature's strong precedent for selecting the zinc(II) ion as the preferred metal center in most hydrolytic enzymes, a particularly intriguing question arises pertaining to the origin of the unusual metal-dependent reactivity displayed by bacterial PDF. High-resolution X-ray structures of all four M(II)−PDFs show extremely similar active sites,[4−8] and thus at first glance do not offer any obvious explanation for the particularly low activity of Zn−PDF. A detailed mechanistic understanding of the differences in reactivity between bacterial Fe(II)− and Zn−PDF is still lacking.

With this question in mind, we have prepared and studied the hydrolytic reactivity of the mononuclear N_2S(thiolate) zinc complex (PATH)ZnOH (**1**), which closely mimics the 2-His/1-Cys coordination environment of the PDF active site. In a previous study, we showed that **1** could be cleanly generated in aqueous solution by dissolution of (PATH)Zn-(CH_3) in H_2O. Potentiometric titration and ^{1}H NMR data showed that **1** remains a mononuclear complex in aqueous solution. The hydrolytic reactivity of **1** toward the carboxylic ester substrate 4-nitrophenyl acetate (4-NA) was found to compare well with other zinc model complexes and enzymes.[14] Kinetic and thermodynamic measurements showed that the reaction between **1** and 4-NA proceeded through a mechanism involving simple nucleophilic attack of the metal-bound hydroxide on the carboxylic ester. The pK_a and associated nucleophilicity of the metal−hydroxide was also found to be in reasonable agreement with other zinc model complexes. A major finding of this previous work was that a Zn(II) ion in an N_2S(thiolate) environment, as found in PDF, exhibits normal hydrolytic activity and associated properties, suggesting that the low reactivity of PDF may come from other, more subtle effects.

Work by others[15−19] on mononuclear zinc model complexes has also shown that the hydrolysis of carboxylic ester substrates proceeds through a simple nucleophilic attack mechanism. In comparison, zinc-promoted hydrolysis of *phosphate* esters usually proceeds via a "hybrid" mechanism, in which the substrate coordinates to the Lewis acidic (L_n)Zn(OH) species, thereby undergoing both Lewis acid activation and intramolecular attack by the metal-bound OH^-.[16,20−23] Vahrenkamp and co-workers have suggested that the hydrolysis of both carboxylic and phosphate ester substrates proceeds via this type of hybrid mechanism, although this proposal was based on studies under non-aqueous conditions.[21]

Herein we have determined the hydrolytic reactivity of **1** toward the phosphate triester substrate tris(4-nitrophenyl) phosphate (TNP). We wanted to compare the reactivity and associated properties (e.g. pK_a and rate constants) for the hydrolysis of TNP with those found previously for the substrate 4-NA,[14] as well as with the parameters found for other zinc model complexes. The TNP substrate was selected in part because it is a well-studied neutral substrate similar to 4-NA and because there are benchmark data in the literature for comparison. In addition, the metal-promoted hydrolysis of phosphate esters is a subject of general interest because of the relevance to naturally occurring phosphatases and the related efforts in developing artificial nucleases.[24]

Our kinetic analysis for the hydrolysis of TNP by **1** points to a hybrid mechanism. These results, combined with our previous data for the hydrolysis of 4-NA, reveal the highly flexible nature of the zinc ion in the PATH ligand environment and show that zinc-promoted hydrolyses can operate through different mechanisms depending on the substrate. These findings are discussed in light of bacterial PDF's unusual metal-dependent reactivity.

The syntheses of Co(II), Ni(II), and especially Fe(II) complexes of PATH are also of interest in light of the Co(II), Ni(II), and Fe(II) forms of PDF. Previously we had described the synthesis and structural characterization of the tetrahedral cobalt(II) complexes (PATH)CoBr and (PATH)Co(NCS) and the generation of (PATH)Co(OH) in methanolic solution.[25] However, Ni(II) or Fe(II) complexes of PATH have not been described up to now. Herein we report the synthesis and structural characterization of the new PATH complexes

(9) (a) Rajagopalan, P. T. R.; Yu, X. C.; Pei, D. *J. Am. Chem. Soc.* **1997**, *119*, 12418−12419. (b) Groche, D.; Becker, A.; Schlichting, I.; Kabsch, W.; Schultz, S.; Wagner, A. F. V. *Biochem. Biophys. Res. Commun.* **1998**, *246*, 342−346.
(10) Serero, A.; Giglione, C.; Meinnel, T. *J. Mol. Biol.* **2001**, *314*, 695−708.
(11) Rajagopalan, P. T. R.; Grimme, S.; Pei, D. *Biochemistry* **2000**, *39*, 779−790.
(12) Ragusa, S.; Blanquet, S.; Meinnel, T. *J. Mol. Biol.* **1998**, *280*, 515−523.
(13) Li, Y.; Chen, Z.; Gong, W. *Biochem. Biophys. Res. Commun.* **2002**, *295*, 884−889.
(14) diTargiani, R. C.; Chang, S. C.; Salter, M. H.; Hancock, R. D.; Goldberg, D. P. *Inorg. Chem.* **2003**, *42*, 5825−5836.
(15) Kimura, E.; Shiota, T.; Koike, T.; Shiro, M.; Kodama, M. *J. Am. Chem. Soc.* **1990**, *112*, 5805−5811.
(16) Koike, T.; Kimura, E. *J. Am. Chem. Soc.* **1991**, *113*, 8935−8941.
(17) Koike, T.; Takamura, M.; Kimura, E. *J. Am. Chem. Soc.* **1994**, *116*, 8443−8449.
(18) Bazzicalupi, C.; Bencini, A.; Bianchi, A.; Fusi, V.; Giorgi, C.; Paoletti, P.; Valtancoli, B.; Zanchi, D. *Inorg. Chem.* **1997**, *36*, 2784−2790.
(19) Xia, J.; Xu, Y.; Li, S. A.; Sun, W. Y.; Yu, K. B.; Tang, W. X. *Inorg. Chem.* **2001**, *40*, 2394−2401.
(20) Bonfá, L.; Gatos, M.; Mancin, F.; Tecilla, P.; Tonellato, U. *Inorg. Chem.* **2003**, *42*, 3943−3949.
(21) Rombach, M.; Maurer, C.; Weis, K.; Keller, E.; Vahrenkamp, H. *Chem.*—Eur. J. **1999**, *5*, 1013−1027.
(22) Itoh, T.; Fujii, Y.; Tada, T.; Yoshikawa, Y.; Hisada, H. *Bull. Chem. Soc. Jpn.* **1996**, *69*, 1265−1274.
(23) Livieri, M.; Mancin, F.; Toneliato, U.; Chin, J. *Chem. Commun.* **2004**, 2862−2863.
(24) (a) Trawick, B. N.; Daniher, A. T.; Bashkin, J. K. *Chem. Rev.* **1998**, *98*, 939−960. (b) Hegg, E. L.; Burstyn, J. N. *Coord. Chem. Rev.* **1998**, *173*, 133−165. (c) Krämer, R. *Coord. Chem. Rev.* **1999**, *182*, 243−261. (d) Blaskó, A.; Bruice, T. C. *Acc. Chem. Res.* **1999**, *32*, 475−484. (e) Williams, N. H.; Takasaki, B.; Wall, M.; Chin, J. *Acc. Chem. Res.* **1999**, *32*, 485−493. (f) Molenveld, P.; Engbersen, J. F. J.; Reinhoudt, D. N. *Chem. Soc. Rev.* **2000**, *29*, 75−86. (g) Iranzo, O.; Richard, J. P.; Morrow, J. R. *Inorg. Chem.* **2004**, *43*, 1743−1750. (h) He, C.; Gomez, V.; Spingler, B.; Lippard, S. J. *Inorg. Chem.* **2000**, *39*, 4188−4189. (i) He, C.; Lippard, S. J. *J. Am. Chem. Soc.* **2000**, *122*, 184−185.
(25) Chang, S. C.; Karambelkar, V. V.; Sommer, R. D.; Rheingold, A. L.; Goldberg, D. P. *Inorg. Chem.* **2002**, *41*, 239−248.

$[(PATH)_2Ni_2]Br_2$ (**2**) and $(PATH)_2Fe_2Cl_2$ (**3**). Both complexes are dinuclear, bis(μ-thiolate) complexes in which the sulfur donor of PATH provides the bridging atoms of an $M_2(\mu\text{-SR})_2$ core. The nickel complex is quite similar to other $Ni_2(\mu\text{-SR})_2$ dimers, but the dinuclear iron(II) complex exhibits a rare asymmetric structural motif in which both iron centers are 5-coordinate.

Experimental Section

General Procedures. PATH-H[25] was prepared as previously described. The complex (PATH)ZnOH (**1**) was generated in aqueous solution by the dissolution of $(PATH)ZnCH_3$ in D_2O as describe previously.[14] A fresh stock solution of **1** was prepared within 1 week of performing kinetic experiments. The concentration of **1** in this stock solution was obtained from NMR integration against an internal standard (NaO_2CCH_3). Tris(4-nitrophenyl) phosphate (TNP) and Good's buffers CHES (2-(cyclohexylamino)-propanesulfonic acid), EPPS (*N*-(2-hydroxyethyl)piperazine-*N*′-3-propanesulfonic acid), and HEPES (*N*-(1-hydroxyethyl)piperazine-*N*′-2-ethanesulfonic acid) were obtained from Sigma and used without further purification. Deuterated compounds D_2O, ethanol-d_6, and NaOD were obtained from Cambridge Isotope Laboratories. Starting materials $NiBr_2$ and $FeCl_2{\cdot}4H_2O$ were obtained from Aldrich. NaO_2CCH_3 and $NaNO_3$ were obtained from J. T. Baker. THF was distilled from sodium/benzophenone prior to use. ^{1}H NMR spectra were recorded on a Bruker AMX-400 spectrometer (400 MHz). Tetramethylsilane in organic solvents and HOD (4.80 ppm) in D_2O were used as internal references for ^{1}H NMR measurements. Kinetic studies were carried out by a visible spectral method using an Agilent 8453 photodiode-array spectrophotometer equipped with a thermostable cell holder and the Agilent biochemical analysis software package.

$[(PATH)_2Ni_2]Br_2$ (2). The sodium thiolate of PATH-H was generated by the addition of NaOH (0.014 g, 0.36 mmol) to a solution of PATH-H (0.075 g, 0.33 mmol) in MeOH (10 mL). Once the NaOH was consumed, the solution was added dropwise to a green solution of $NiBr_2$ (0.073 g, 0.33 mmol) in MeOH (50 mL). The resulting green solution was stirred for 15 h. Upon reduction of the volume of the solution under vacuum, a dark red precipitate formed. The mixture was filtered, and the precipitate was washed with cold diethyl ether and dried under vacuum. For X-ray diffraction studies, dark red crystals of $[(PATH)_2Ni_2]Br_2{\cdot}CH_3OH$ were obtained by vapor diffusion of diethyl ether into a solution of the complex in MeOH. A fine white solid precipitated during crystal formation, which could be removed from the large red crystals by suspension in diethyl ether and decantation of the ether layer. Anal. Found: C, 39.42; H, 5.53; N, 7.35. Calcd for $C_{24}H_{38}N_4Br_2Ni_2S_2$: C, 39.82; H, 5.29; N, 7.74.

$(PATH)_2Fe_2Cl_2$ (3). The sodium thiolate of PATH-H was generated by the addition of NaOH (0.071 g, 1.8 mmol) to a solution of PATH-H (0.36 g, 1.6 mmol) in MeOH (10 mL). Once the NaOH was consumed, the solution was added dropwise to a yellow solution of $FeCl_2{\cdot}4H_2O$ (0.31 g, 1.6 mmol) in MeOH (30 mL). The resulting yellow solution was stirred for 2 h and filtered. The filtrate was dried under vacuum to give a yellow powder that was redissolved in a minimum amount of acetonitrile. A yellow crystalline solid precipitated from the CH_3CN solution after the addition of diethyl ether. The yellow solid was redissolved in CH_2Cl_2, and slow vapor diffusion of diethyl ether led to the formation of dark red-brown crystals of **3**. Anal. Found: C, 45.74; H, 6.04; N, 8.87. Calcd for $C_{24}H_{38}N_4Cl_2Fe_2S_2$: C, 45.81; H, 6.09; N, 8.90.

X-ray Crystallography. Crystallography data and details of X-ray studies for **2** and **3** are given in Table 1. Data were collected at 173 K on a Bruker Smart Apex CCD diffractometer using Mo Kα radiation ($\lambda = 0.710\,73$ Å). Absorption corrections were applied for all data by SADABS.[26] Non-hydrogen atoms in both structures were refined with anisotropic displacement coefficients. The H atoms were treated as idealized contributions. Crystals of **3** were extremely air-sensitive and decayed during data collection. Data quality declined after ~70% of the reflections were collected, and therefore, data collection was stopped at this point. All software and sources of scattering factors are contained in the SHELXTL (5.10) program package.[27]

Table 1. Crystallographic Data and Details of X-ray Studies for Complexes **2** and **3**

param	**2**·CH_3OH	**3**
empirical formula	$C_{25}H_{42}Br_2N_4Ni_2OS_2$	$C_{24}H_{38}Cl_2Fe_2N_4S_2$
M_r	775.99	629.30
cryst size (mm)	0.30 × 0.30 × 0.10	0.50 × 0.40 × 0.28
cryst system	monoclinic	triclinic
space group	$P2/n$	$P\bar{1}$
a, Å	11.2082(17)	9.232(3)
b, Å	6.2933(9)	9.634(3)
c, Å	21.808(3)	16.524(5)
α, deg	90	93.439(17)
β, deg	102.352(3)	94.924(18)
γ, deg	90	107.698(17)
V, Å^3	1502.7(4)	1389.2(7)
Z, Z'	2, 0.5	2, 1
ρ_{calcd}, g/cm^3	1.671	1.504
μ, mm^{-1}	4.077	1.408
measd reflcns	6321	9485
R_{int}	0.0356	0.0376
indep reflcns	3040	5093
abs corr	SADABS	SADABS
T_{min}/T_{max}	0.546	0.778
T, K	173(2)	173(2)
R1,[a] wR2[b] (all data)	0.0527, 0.1280	0.0811, 0.1762
R1,[a] wR2[b] [$I > 2\sigma(I)$]	0.0441, 0.1194	0.0566, 0.1333
GOF on F^2	0.976	1.129

[a] $R = \Sigma||F_o| - |F_c||/\Sigma|F_o|$. [b] $R(wF^2) = \{\Sigma[w(F_o^2 - F_c^2)^2]/\Sigma[w(F_o^2)^2]\}^{1/2}$.

Hydrolysis of TNP. Product Analysis. To 4.15 mg of TNP in an NMR tube was added 100 μL of D_2O followed by (PATH)-ZnOH (300 μL of 30 mM stock solution in D_2O) and 200 μL of ethanol-d_6. The pH was set to 8.4 with NaOD. To increase the solubility of TNP, it was necessary to warm the solution to 40 °C prior to collecting the ^{1}H NMR spectrum. A small amount of undissolved TNP was still present in the NMR tube. After 20 h, the ^{1}H NMR spectrum showed peaks corresponding to (PATH)-ZnOH and the hydrolysis products 4-nitrophenolate (4-NP) and bis(4-nitrophenyl) phosphate (BNP). No other peaks were observed.

Hydrolysis of TNP. Kinetics. The rate of hydrolysis of TNP promoted by (PATH)ZnOH in H_2O/EtOH (66:33 v/v) in the pH range 7.0−10.0 was measured under pseudo-first-order conditions. The reaction was monitored by following the increase in absorbance at 405 nm, corresponding to the appearance of the product 4-NP, until 90% completion (4−5 half-lives). The pH was maintained by using HEPES (pH 7.0−8.1), EPPS (pH 8.2−8.5), or CHES (pH 8.6−10.0) buffer at 10 mM. The pH values in 33% ethanol were corrected by subtracting 0.09 from all readings from the pH meter.[28] Ionic strength was maintained by $NaNO_3$ at 100 mM. The temperature was monitored by a thermocouple inserted directly into the UV−vis cell and shown to vary no more than ±0.5 °C

(26) Sheldrick, G. M. *SADABS (2.01), Bruker/Siemens Area Detector Absorption Correction Program*; Bruker AXS: Madison, WI, 1998.
(27) Sheldrick, G. M. *SHEXTL: Program Package for Structure Solution and Refinement*; Bruker AXS: Madison, WI, 1997.
(28) Bates, R. G.; Paabo, M.; Robinson, R. A. *J. Phys. Chem.* **1963**, *67*, 1833−1838.

throughout the kinetics run. A typical experiment consisted of loading a UV−vis cell (3.0 mL total volume) with 1.0 mL of ethanol, 1.0 mL of a stock solution containing the appropriate buffer and $NaNO_3$ (30 mM and 300 mM, respectively), and 1.0 mL of a stock solution of (PATH)ZnOH (3 mM). The reaction was initiated by injecting 15 μL of a stock solution of TNP (1 mM in dry THF). The stock solution of (PATH)ZnOH used in the kinetic runs was prepared within 1 week of taking measurements to avoid any decomposition. The concentration of (PATH)ZnOH was varied (0.1−3.0 mM) with constant [TNP] (0.005 mM). Plots of *A*(405 nm) vs time showed good first-order behavior, and the exponential growth curves were fitted to the appropriate equation (see Results and Discussion) to give the observed rate constants, k_{obs} (s^{-1}). Second-order rate constants k'' (M^{-1} s^{-1}) were determined from the slopes of best-fit lines for plots of k_{obs} vs $[(PATH)Zn]_{total}$, where $[(PATH)Zn]_{total} = [(PATH)ZnOH] + [(PATH)Zn(OH_2)]$. Good linearity was observed in these plots at all pH values. The background reaction rate constant (no metal complex present), k_{buffer}, was measured at all pH values by loading the UV−vis cell with all of the reagents as described above with the exception of **1**, which was replaced by an equal amount of distilled water. Background hydrolysis of TNP was shown to range from $k_{buffer} = 1.00 \times 10^{-3}$ s^{-1} at pH 7.0 to 1.25×10^{-3} s^{-1} at pH 9.4. The *y*-intercepts of the k_{obs} vs $[(PATH)Zn]_{total}$ plots were similar to the measured k_{buffer}, as expected. Due to their independence from the *y*-intercept, the values of the second-order rate constants, k'', were not adjusted for background hydrolysis. At each pH, and for each $[(PATH)Zn]_{total}$ value, the k_{obs} value was obtained at least in duplicate and is reported as an average of these measurements, with a variation in k_{obs} of ±10%.

Temperature Dependence of the Hydrolysis of TNP. The effect of temperature on the hydrolysis of TNP was determined at pH 8.0 over a temperature range 25−60 °C. Reactions were performed in HEPES buffer (10 mM) with an ionic strength of 0.1 M maintained by $NaNO_3$. The reactions were run in a UV−vis cell as described in the kinetics section. In a typical experiment, the temperature of the UV−vis cell loaded with the (PATH)ZnOH complex was set by a circulating water bath and allowed to equilibrate for 5 min. The reaction was then initiated by injecting 15 μL of TNP (1 mM in dry THF) into the UV−vis cell. The temperature was monitored by a thermocouple inserted directly into the UV−vis cell and shown to vary no more than ±0.3 °C throughout the kinetic run.

Results and Discussion

Phosphotriester Hydrolysis Promoted by (PATH)ZnOH. The substrate TNP was chosen in part because it is a neutral phosphate triester, as opposed to the monoanionic diester bis(nitrophenyl) phosphate (BNP) or dianionic mononitrophenyl phosphate (MNP). It therefore has the same charge as the previously studied neutral 4-NA,[14] as well as the native formyl substrate of PDF. Thus the preference for coordination to zinc(II) by these different substrates can be compared without complications from differences in charge.

Hydrolysis of TNP. Product Analysis. The hydrolysis of TNP was carried out in a mixture of water/ethanol (66:33 v/v) because this solvent system is the best one for solubility. Initial attempts were made to run the hydrolysis in H_2O/CH_3CN (90:10), since this mixture was used for the previous study of 4-NA,[14] but precipitates formed under these conditions.

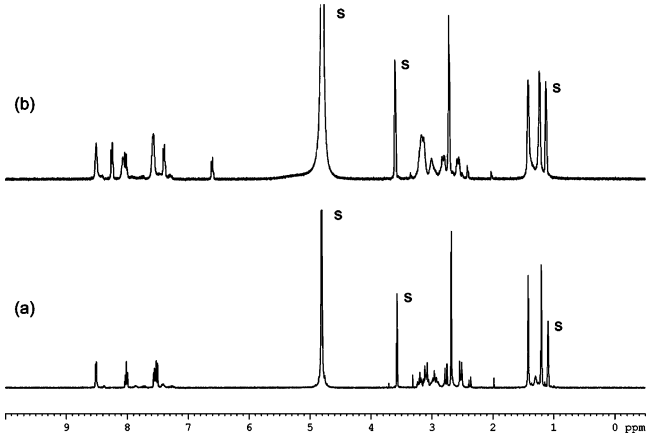

Figure 1. ^1H NMR spectra in D_2O/ethanol-d_6 (66:33 v/v) at 25 °C of (a) (PATH)ZnOH and (b) (PATH)ZnOH + TNP after 20 h. pH = 8.4. Solvent peaks are marked with an "S".

The reaction between (PATH)ZnOH and TNP was first analyzed by ^1H NMR spectroscopy to identify all of the products formed. The ^1H NMR spectrum of the reaction mixture after complete hydrolysis of TNP is shown in Figure 1, along with the spectrum of (PATH)ZnOH in the same solvent system (D_2O/ethanol-d_6, 66:33 v/v).

There are three sets of peaks in the aromatic region that can be clearly distinguished: one set of pyridyl protons at 8.51, 8.02, and 7.57 ppm corresponding to (PATH)ZnOH; two doublets at 8.25 and 7.40 ppm corresponding to BNP; another set of doublets at 8.07 and 6.60 ppm assigned to the 4-NP product. The NMR spectra of BNP and 4-NP were independently measured in D_2O/ethanol-d_6 (66:33 v/v), and comparison of these spectra provides assignments for the reaction mixture. There is no evidence that either BNP or 4-NP coordinate to the PATH−zinc complex, since the peaks in the reaction mixture for (PATH)ZnOH, BNP, and 4-NP are unperturbed from their independent spectra. There is also no indication of a coordinated TNP−zinc complex, but the limited solubility of TNP prevents the observation of this species by NMR. The NMR data indicate that the smooth hydrolysis of TNP is promoted by (PATH)ZnOH as described by the reaction shown in Scheme 1.

Kinetics. The hydrolysis of TNP was conveniently monitored by following an increase in absorbance at 405 nm corresponding to the production of 4-nitrophenolate. Kinetics were followed under pseudo-first-order conditions with the zinc complex as the excess component. The TNP concentration was set to 5.0×10^{-6} M, while the zinc complex concentration was varied between 0.1×10^{-3} and 3.0×10^{-3} M, depending on pH. Clean single-exponential kinetics were observed, as seen in a representative plot of A_{405nm} versus time in Figure 2.

Good fits to the exponential curves were obtained by using the model for exponential growth, given in eq 2, where A_{405} is the absorbance over time at 405 nm and A_f is the final absorbance. Linearity up to 4−5 half-lives was observed for the natural log plot of the same data (inset of Figure 2), verifying pseudo-first-order behavior. A pseudo-first-order rate constant, k_{obs}, was obtained from fitting the exponential curve directly, and several k_{obs} values were measured over a

Scheme 1

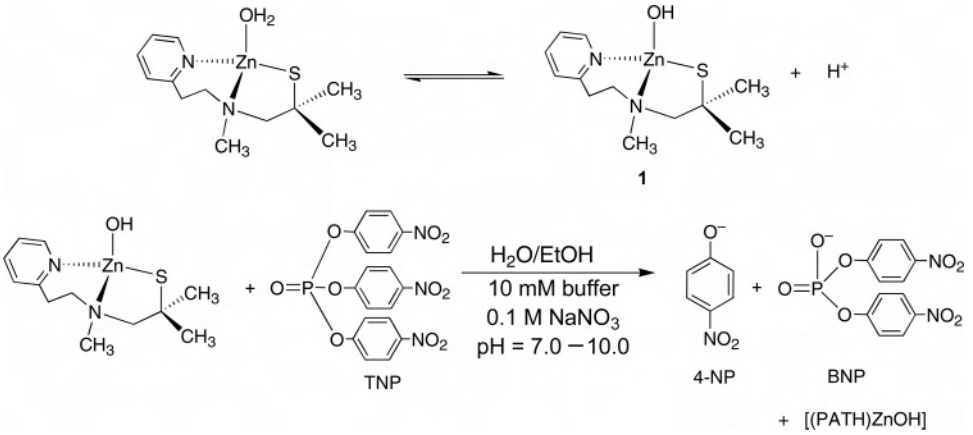

range of concentrations for the zinc complex. Plots of k_{obs} versus zinc complex concentration for three different pH values are shown in Figure 3.

$$A_{405} = A_f(1 - e^{-kt}) \quad (2)$$

The linearity of these graphs shows that the reaction is first-order in zinc complex, leading to the overall second-order rate law shown in eq 3.

The second-order rate constant, k'', was calculated at different pH values from the slopes of the best-fit lines, as shown in Figure 3, and the *y*-intercept provides a measure of the background rate of hydrolysis of TNP in the absence of zinc complex. Independent measurement of the background rate of hydrolysis of TNP at the different pH values was in good agreement with that obtained from linear regression. These values ranged from 1.00×10^{-3} s^{-1} at pH 7.0 to 1.25×10^{-3} s^{-1} at pH 9.4. Comparing the latter value to k_{obs} of 15.3×10^{-3} s^{-1} for 1.0 mM zinc complex at pH 9.4 shows that the zinc complex gives a rate enhancement of about 12 times the background rate. This rate enhancement is strikingly similar to that observed by Kimura,[16] who observed a rate enhancement of ~13 times the background rate of hydrolysis of TNP by the zinc complex of [12]aneN$_3$ (Chart 1).

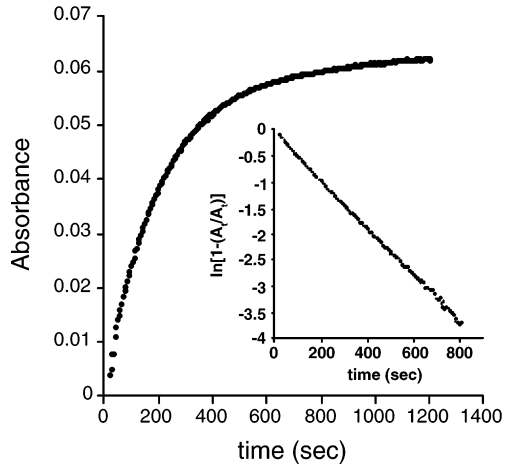

Figure 2. Hydrolysis of TNP in EtOH/H_2O (33:66 v/v) at pH 8.0 (10 mM HEPES, I = 0.1 M $NaNO_3$) monitored by UV−vis spectroscopy at λ_{max}(4-NP) = 405 nm. Initial concentration of TNP = 0.005 mM and of $[(PATH)Zn]_{total}$ = 1.0 mM, where $[(PATH)Zn]_{total}$ = [(PATH)ZnOH] + $[(PATH)Zn(OH_2)]^+$. Inset: Plot of $\ln(1 - (A_t/A_f))$ versus time for the same data, where A_t is the absorbance at a given time and A_f is the final absorbance.

$$\text{rate} = k''[(PATH)Zn]_{total}[TNP] \quad (3)$$

Dependence of the Hydrolysis of TNP on pH. A graph of k'' values versus pH is shown in Figure 4. This pH−rate profile shows that the hydrolysis of TNP is accelerated by an increase in pH, consistent with a deprotonation event preceding the hydrolysis step and implicating the zinc−hydroxide complex as the active hydrolytic species.

The expression in eq 4 was used to fit the pH−rate profile, derived from the mechanism corresponding to Scheme 1, which shows a single deprotonation equilibrium preceding the rate-determining-step.[29]

$$k'' = k''_{max}K_a/(K_a + [H^+]) \quad (4)$$

In eq 4, k''_{max} represents the pH-independent rate constant and corresponds to the rate constant for the second step in Scheme 1, while K_a is the equilibrium constant for the first step. Thus k''_{max} provides a measure of the inherent reactivity of the hydroxide complex. A similar pH-rate profile was obtained for the hydrolysis of the carboxylic ester 4-NA by (PATH)ZnOH.[14]

The k''_{max} and pK_a values for (PATH)ZnOH are given in Table 2 together with some literature data. The kinetically determined pK_a for (PATH)ZnOH in this study is in reasonable agreement with that determined previously from the kinetics of hydrolysis of 4-NA (pK_a = 8.05(5)) as well as potentiometric titration (pK_a = 7.7(1), in H_2O/CH_3CN) of the PATH−zinc system in H_2O. The change in solvent system (H_2O/CH_3CN versus H_2O/EtOH) may account for the slight differences in the pK_a.

The data in Table 2 show that **1** is the most reactive zinc(II) complex determined thus far toward the hydrolysis of TNP. Only a recently reported dinuclear copper(II)

(29) Zuman, P.; Patel, R. C. *Techniques in Organic Reaction Kinetics*; John Wiley & Sons: New York, 1984.
(30) Ibrahim, M. M.; Shimomura, N.; Ichikawa, K.; Shiro, M. *Inorg. Chim. Acta* **2001**, *313*, 125−136.
(31) Clewley, R. G.; Slebocka-Tilk, H.; Brown, R. S. *Inorg. Chim. Acta* **1989**, *157*, 233−238.

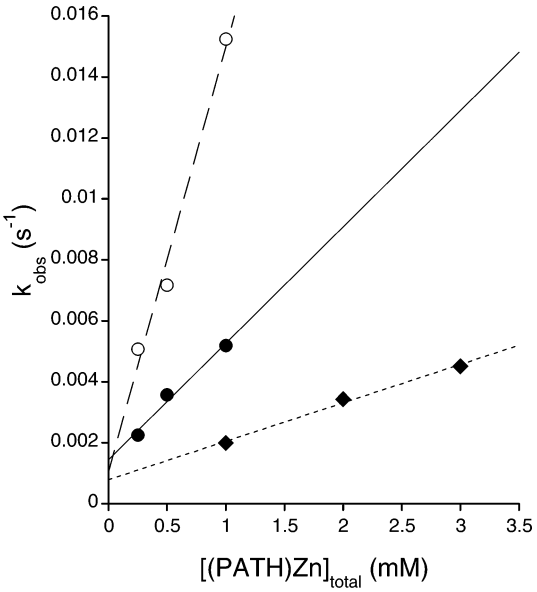

Figure 3. Dependence of k_{obs} on $[(PATH)Zn]_{total}$ for the hydrolysis of TNP in EtOH/H_2O (33:66 v/v) at three representative pH values (10 mM HEPES or CHES, $I = 0.1$ M $NaNO_3$). The k'' value is obtained from the slope of the best-fit line. Key: pH 7.2 (■), $k'' = 1.26$ M^{-1} s^{-1}; pH 8.0 (●), $k'' = 3.81$ M^{-1} s^{-1}; pH 9.4 (○), $k'' = 12.5$ M^{-1} s^{-1}.

Chart 1

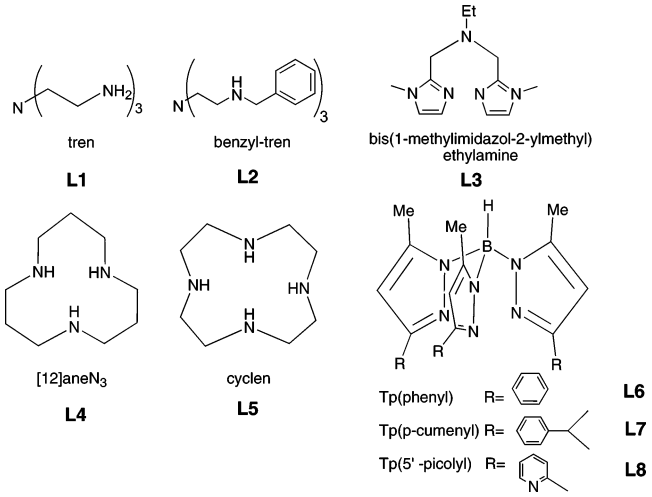

complex exhibits a higher second-order rate constant (28.1 M^{-1} s^{-1} at pH 10), and this is one of the most active complexes known for promoting the hydrolysis of TNP in an aqueous environment.[32] However, the rate constant for the PATH complex is only somewhat larger than that found for ([12]aneN$_3$)ZnOH or (benzyltren)ZnOH (Chart 1), and variations in the conditions (e.g. solvent, buffer, method of kinetic analysis) employed in these studies may contribute to the differences in rate constant.

Despite this caveat, the PATH complex clearly exhibits high activity toward TNP, and most importantly, k''_{max} is slightly higher than that reported[16] for free OH^- ion (we independently measured k''_{max}(free OH^-), and it was in good agreement with the literature value). In contrast, the k''_{max} value obtained for the hydrolysis of 4-NA mediated by (PATH)ZnOH, 8.9(3) × 10^{-2} M^{-1} s^{-1}, is significantly smaller than that for free OH^- ion (9.5 M^{-1} s^{-1}).[33]

As has been pointed out by others,[16,34] the relative

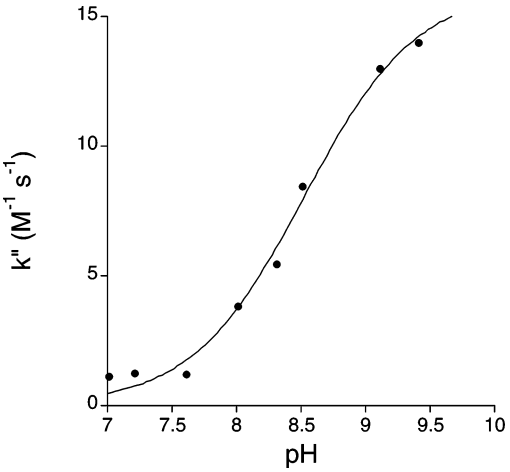

Figure 4. Dependence of k'' on pH for the hydrolysis of TNP in EtOH/H_2O (33:66 v/v) with $I = 0.1$ M $NaNO_3$ and 10 mM HEPES, CHES, or EPPS. The line represents the best fit of the data to eq 4.

Table 2. Comparison of the pK_a Values and Second-Order Rate Constants k''_{max} (M^{-1} s^{-1}) for Hydrolysis of TNP Promoted by Mononuclear (L)Zn^{II} Complexes and Free OH^-

	pK_a	k''_{max} (M^{-1} s^{-1})	ref
OH^-	15.7	10.7 ± 0.2[a]	16
ligand (L)			
PATH	8.52(5)	16.1(7)	this work
L1	10.72[b]	6[b,c]	30
L2	9.61[b]	11[b,c]	30
L3	8.3[a]	3.7[a]	31
L4	7.2	7.0 ± 0.2[b]	16
L5	7.9	3.7 ± 0.2[b]	16
L6		1.545[d]	21
L7		0.452[d]	21
L8		1.090[d]	21

[a] Measured in H_2O/EtOH (66/33 v/v), $T = 25.0$ °C. [b] Measured in H_2O/MeOH (66/33 v/v), 0.1 M $NaNO_3$. [c] Calculated for pH 11 using $k'' = k_{obs}$/[Zn complex], where k_{obs} is a pseudo-first-order rate constant. [d] Measured in $CHCl_3$, $T = 25.0$ °C.

reactivity of metal-promoted hydrolysis versus free OH^- provides significant insight regarding mechanism. The nucleophilicity of a metal-bound hydroxide must be lower than free OH^- ion on the basis of simple charge and steric considerations. Therefore, a mechanism relying on simple nucleophilic attack of the metal-bound hydroxide, as shown in Scheme 2a, necessarily implies a smaller k''_{max} than free OH^-. We previously concluded that such a mechanism was operative for the reaction between **1** and 4-NA, in keeping with the order of rate constants k''_{max}((PATH)ZnOH) ≪ k''_{max}(OH^-). For TNP, this same argument clearly disfavors the simple nucleophilic attack mechanism, and therefore Scheme 2a is not a reasonable choice for the hydrolysis of TNP.

The high reactivity of **1** toward TNP can be rationalized via the hybrid mechanism shown in Scheme 2b. In this mechanism, nucleophilic attack of the metal-bound hydroxide takes place while the substrate is coordinated to the metal ion through the phosphoryl oxygen atom. This mechanism

(32) Itoh, M.; Nakazawa, J.; Maeda, K.; Kano, K.; Mizutani, T.; Kodera, M. *Inorg. Chem.* **2005**, *44*, 691−702.
(33) Jencks, W. P.; Gilchrist, M. *J. Am. Chem. Soc.* **1968**, *90*, 2622−2637.
(34) Gellman, S. H.; Petter, R.; Breslow, R. *J. Am. Chem. Soc.* **1986**, *108*, 2388−2394.

Scheme 2. Possible Mechanisms of Hydrolysis of TNP

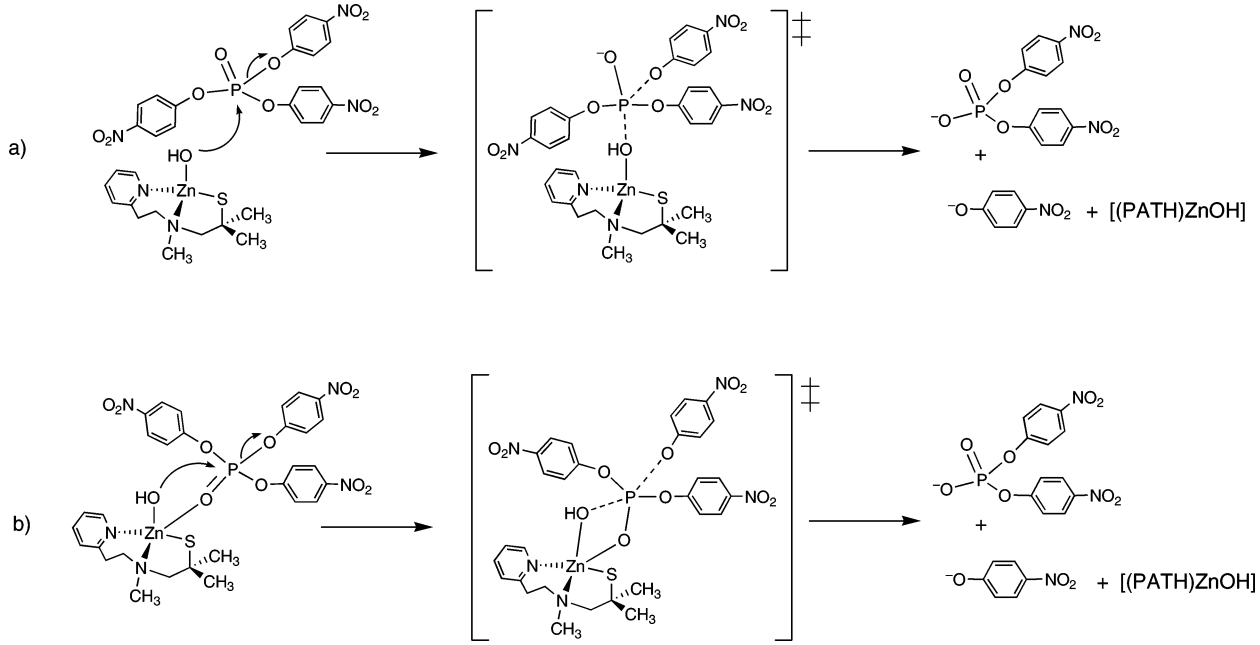

is consistent with k''_{max}((PATH)ZnOH) > k''_{max}(OH^-), since the combined effects of Lewis acid activation of the substrate and nucleophilic attack of the Zn−OH unit effectively lowers the energy of the transition state. Direct coordination of the substrate to zinc also induces a proximity effect between the substrate and OH^-. These combined effects, which are typical for enzyme-catalyzed reactions, account for the better hydrolytic efficiency of (PATH)ZnOH as compared to free OH^-.

A similar conclusion was reached by Kimura regarding the cyclen and [12]aneN_3 complexes in Table 2, for which a hybrid mechanism was invoked for the hydrolysis of neutral TNP as well as for the monoanionic diester BNP.[16] Kimura found that hydrolysis of BNP was significantly enhanced compared to free OH^-, while for TNP the hydrolysis was close to, but slightly less efficient than, free OH^-. It was therefore concluded that "more hybrid trend" was operative for anionic phosphates (e.g. BNP^-), while "less hybrid trend" was operative for neutral phosphates (e.g. TNP).[16] However, a recent study by Mancin and co-workers suggested that $(L)Zn^{II}$-mediated hydrolysis of a phosphate triester was more affected than a phosphate diester by Lewis acid activation.[20] This suggestion was based on the argument that, for a phosphate triester, the developing negative charge on the phosphoryl oxygen atom would be stabilized by direct coordination to zinc, whereas for a diester the developing negative charge would be localized on an oxygen atom that is not coordinated to the metal ion. The high k''_{max} value for (PATH)ZnOH, especially in comparison to free OH^-, is in keeping with this argument.

Outside of zinc-promoted hydrolysis, not much information is available regarding neutral phosphate triesters, but detailed mechanistic work by Burstyn and co-workers on the hydrolysis of phosphate diesters with the labile mononuclear copper complex $[(TACN)Cu^{II}(OH)(OH_2)]^+$ has revealed a hybrid mechanism.[35,36] In addition, several studies on inert mononuclear metal complexes (e.g. La(III), Co(III), Ir(III)) hydrolyzing phosphate diester substrates has revealed a mechanism involving coordination of the substrate followed by intramolecular nucleophilic attack.[37−43]

The hybrid mechanism of Scheme 2b implies that saturation kinetics should be observable. We attempted to look for Michaelis−Menten behavior by adding excess TNP to the PATH−zinc complex but were severely limited by the solubility properties of TNP. The solubility of TNP was found to be ∼0.04 M in pure THF, and upon addition of this stock solution to the H_2O/EtOH system needed for kinetics, the solubility dropped to $\sim 2.5 \times 10^{-5}$ M. This concentration level was not practical for obtaining the initial rate data necessary to construct a Michaelis−Menten curve. In fact, few studies of mononuclear zinc complexes involved in the hydrolysis of phosphate or carboxylic esters have reported saturation behavior.[44] Although for monoanionic diesters such as BNP solubility in aqueous solutions is less of problem, saturation behavior is still usually not observed because of the very weak binding constants of phosphate diesters to Zn(II) complexes ($K < 0.5\ M^{-1}$).[16,20]

Inspection of the data in Table 2 shows that there is no correlation between the pK_a of the metal-bound hydroxide and second-order rate constants, as opposed to the trend found for the hydrolysis of 4-NA.[14] Thus, the nucleophilicity

(35) Deal, K. A.; Hengge, A. C.; Burstyn, J. N. *J. Am. Chem. Soc.* **1996**, *118*, 1713−1718.
(36) Deal, K. A.; Burstyn, J. N. *Inorg. Chem.* **1996**, *35*, 2792−2798.
(37) Hendry, P.; Sargeson, A. M. *Inorg. Chem.* **1990**, *29*, 92−97.
(38) Hendry, P.; Sargeson, A. M. *Prog. Inorg. Chem.* **1990**, *38*, 201−258.
(39) Hendry, P.; Sargeson, A. M. *J. Am. Chem. Soc.* **1989**, *111*, 2521−2527.
(40) Chin, J.; Zou, X. *J. Am. Chem. Soc.* **1988**, *110*, 223−225.
(41) Chin, J.; Banaszczyk, M.; Jubian, V.; Zou, X. *J. Am. Chem. Soc.* **1989**, *111*, 186−190.
(42) Morrow, J. R.; Buttrey, L. A.; Shelton, V. M.; Berback, K. A. *J. Am. Chem. Soc.* **1992**, *114*, 1903−1905.
(43) Morrow, J. R.; Buttrey, L. A.; Berback, K. A. *Inorg. Chem.* **1992**, *31*, 16−20.
(44) Sprigings, T. G.; Hall, C. D. *J. Chem. Soc., Perkins Trans. 2* **2001**, 2063−2067.

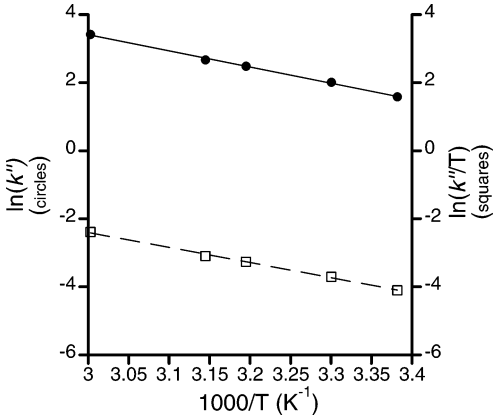

Figure 5. Effect of temperature on the hydrolysis of TNP in EtOH/H_2O (33:66 v/v): ln k'' vs $1000/T$ (●); ln k''/T vs $1000/T$ (□). Conditions: pH 8.0; 10 mM HEPES; $I = 0.1$ M $NaNO_3$. Initial concentration of TNP = 0.005 mM and of $[(PATH)Zn]_{total} = 1.0$ mM.

of M−OH, inasmuch as it is approximated by the pK_a values, is not the controlling factor in the hydrolytic efficiency, providing further evidence against Scheme 2a as the operative mechanism. Invoking Scheme 2b points to three competing factors that control the reactivity: the nucleophilicity of the metal-bound hydroxide; the Lewis acidity of the zinc ion; the availability of a binding site on the zinc center. The nucleophilicity of M−OH necessarily decreases with increasing Lewis acidity (lower pK_a), and there is a balance at play that determines the ultimate hydrolytic reactivity toward a particular substrate. In addition, the coordination number and flexibility of the polydentate ligand will determine the availability of a binding site on the zinc ion. Given these subtle, competing effects, it is not surprising that there is no discernible pattern regarding the rate constants and complexes in Table 2. It has been shown by Kimura that the zinc complex of the tridentate ligand [12]aneN_3 has a *lower* pK_a but is *more reactive* toward organophosphate triesters than a more crowded zinc complex of a tetradentate ligand with a higher pK_a.[16] The high reactivity of (PATH)-ZnOH is likely due to an appropriate combination of the former factors, determined by the properties of the PATH ligand. A reasonably high nucleophilicity is induced by PATH, while the three-coordinate, flexible nature of this ligand allows access to the metal center for substrate activation.

Activation Parameters. The temperature dependence of the second-order rate constants was determined at pH 8.0 and is shown in Figure 5. Good linear behavior is shown for both Arrhenius and Eyring plots over the temperature range 25−60 °C, and linear fits of these plots gave activation parameters of $E_a = 39.5(1)$ kJ mol^{-1}, $\Delta H^{\ddagger} = 36.9(1)$ kJ mol^{-1}, and $\Delta S^{\ddagger} = -106.7(4)$ J mol^{-1} K^{-1}. It should be noted that these parameters are derived from the effects of temperature on apparent second-order rate constants that are composites of the $Zn(OH_2)^+$/ZnOH + H^+ equilibrium, the binding of substrate, and the intramolecular attack of the nucleophilic hydroxide on the coordinated phosphorus center. However, the $Zn(OH_2)^+$/ZnOH equilibrium is likely to be extremely fast, as are ligand exchange rates for zinc and, thus, the on/off rates for binding of TNP. Hence it is assumed that the temperature dependence of the rate constants in Figure 5 is mostly due to the rate-limiting step involving intramolecular nucleophilic attack on TNP, proceeding through the transition state in Scheme 2b. Similar assumptions regarding the activation parameters for copper-promoted hydrolysis of phosphate diesters have been made previously.[35]

There are not many data available regarding the activation parameters for zinc-promoted phosphate ester hydrolysis. A notable exception is the work of Vahrenkamp and coworkers, who reported $E_a = 45.8-52.9$ kJ mol^{-1}, $\Delta H^{\ddagger} = 43.3-50.4$ kJ mol^{-1}, and $\Delta S^{\ddagger} = -81$ to -98 J mol^{-1} K^{-1} for the hydrolysis of TNP promoted by tris(pyrazolyl)borate−zinc complexes in organic solvent.[21] It was concluded in this study that the hydrolysis of TNP proceeded via a hybrid mechanism, based largely on the negative entropy of activation, which was taken as evidence for an ordered, four-centered transition state as seen in Scheme 2b. In our case, the $\Delta S^{\ddagger}$ is of similar magnitude and negative in sign, also consistent with significant order in the transition state.

The transition state in Scheme 2b assumes a concerted mechanism in which the attack of the OH^- group occurs simultaneously with the cleavage of the nitrophenolate bond. An associative mechanism is possible that does not involve departure of the leaving group in the transition state and instead involves the formation of a pentavalent phosphorus (phosphorane) intermediate, in which the metal-bound hydroxide has formed a bond with the phosphorus center but the nitrophenolate O−P bond is still intact. This intermediate would then expel the leaving group in a second step. A concerted mechanism for the related copper-promoted hydrolysis of phosphate diesters was established by the elegant isotope effect studies of Burstyn.[35] Both pathways are consistent with the data and conclusions presented here, since either the concerted or associative pathway involves substrate activation in conjunction with nucleophilic attack.

Synthesis of Ni(II) and Fe(II) Complexes. The syntheses of the PATH−nickel(II) and −iron(II) complexes are shown in Scheme 3.

In the synthesis of the nickel complex **2**, addition of PATH to $NiBr_2$ causes a color change from light green to red-brown. A red-brown powder is isolated and recrystallized from MeOH/Et_2O to give dark red, X-ray-quality crystals of **2**. A white precipitate typically deposits from the solution together with the large, red crystals of **2**, and removal of this white impurity was best done by washing the crystals with Et_2O and decanting the Et_2O layer.

For the iron(II) complex **3**, addition of PATH to a solution of $FeCl_2$ in MeOH leads to the formation of a bright yellow solution, which yields a bright yellow crystalline powder after addition of diethyl ether. The yellow solid was characterized by elemental analysis and gave results consistent with the formula Na[(PATH)$FeCl_2$], indicating that this material was possibly a five-coordinate iron(II) complex with two chloride ligands. Repeated attempts to crystallize this yellow complex for X-ray studies led to either no crystalline material or, in the case of CH_2Cl_2/Et_2O, the slow formation of dark brown crystals that gave the dinuclear structure shown in Scheme

Scheme 3. Synthesis of $[(PATH)_2Ni_2]Br_2$ and $(PATH)_2Fe_2Cl_2$

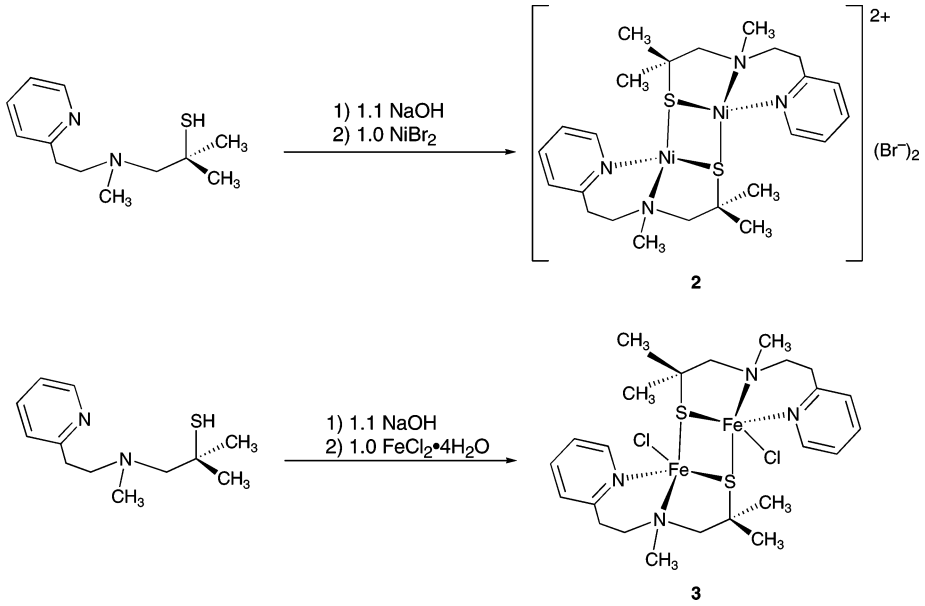

3. The mononuclear yellow complex unfortunately could not be definitively characterized.

Structural Studies. The ORTEP diagrams of **2** and **3** are shown in Figures 6 and 7 with their atomic numbering schemes. Selected bond distances and angles of **2** and **3** are shown in Tables 3 and 4. The structure of the nickel complex reveals two nickel(II) ions coordinated in a square planar environment by the N, N, S donors from PATH and a fourth ligand from a bridging thiolate donor. The overall charge on the complex is +2, and there are two Br^- counterions in the crystal lattice. The $Ni_2(\mu\text{-SR})_2$ core is a common structural motif in Ni(II) chemistry. Although the *gem*-dimethyl groups of PATH help to inhibit thiolate-bridged structures in the case of mononuclear zinc(II) and cobalt(II) complexes, these groups clearly do not impose enough steric hindrance to prevent dimer formation for the Ni(II) ion. The Ni_2S_2 core is not planar, being folded along the S---S vector with a fold angle of 136.5°, measured between the best-fit planes of the nickel coordination spheres. The Ni---Ni distance is 3.065 Å. These structural features are quite similar to the related dinuclear nickel(II) complex $[(mmp\text{-}dach)_2Ni_2][BarF]_2$ prepared by Grapperhaus, Darensbourg, and coworkers, where mmp-dach is a tridentate N_2S(thiolate) ligand, and the fold angle and Ni---Ni distance are 135.7° and 3.034 Å, respectively.[45] It was pointed out that these parameters are larger than for other $Ni_2(\mu\text{-SR})_2$ dimers (fold angle ~ 110°, d(Ni---Ni) = 2.7−2.9 Å),[46,47] and molecular modeling studies suggested that steric encumbrance imposed by the *gem*-dimethyl substituents on the carbon α to the sulfur donor in the mmp-dach ligand was responsible for these structural deviations. Thus, similar steric effects from the *gem*-dimethyl groups in PATH are likely responsible for the obtuse fold angle and long metal−metal distance in **2**. The Ni−N bond lengths are similar to each other (1.920(4) and 1.983(3) Å) and are comparable to those in other N,S−nickel(II) complexes.[45,48] The Ni−S bond lengths are also similar (2.1665(11) and 2.1908(9) Å) and close to the Ni−S distances reported for other Ni(II) complexes.[45,48]

The iron(II) complex **3** is also a bis(thiolate)-bridged complex but exhibits an unusual, unsymmetrical structure. Both iron(II) ions are chelated by the PATH ligand in the

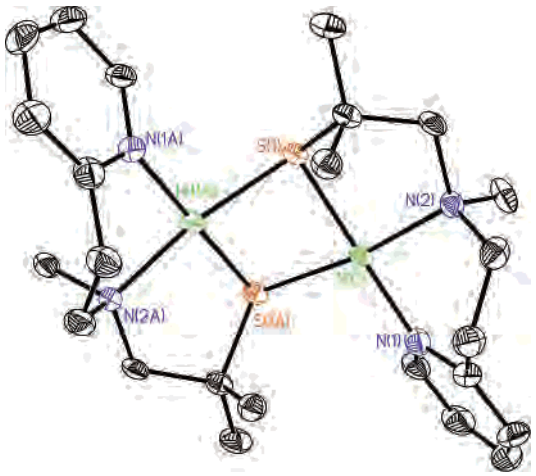

Figure 6. ORTEP diagram showing the 50% probability thermal ellipsoids of $[(PATH)_2Ni_2]^{2+}$ for all non-hydrogen atoms.

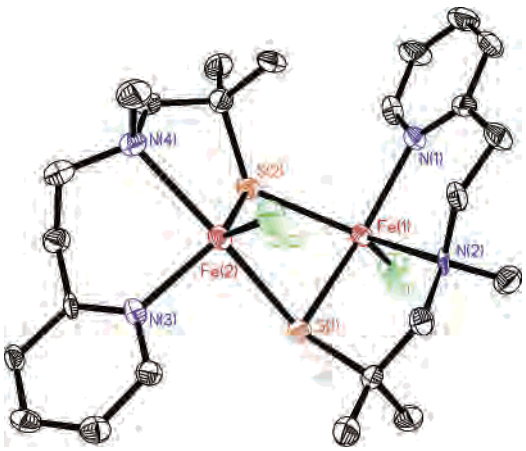

Figure 7. ORTEP diagram showing the 50% probability thermal ellipsoids of $(PATH)_2Fe_2Cl_2$ for all non-hydrogen atoms.

Table 3. Selected Bond Distances (Å) and Angles (deg) for $[Ni^{II}_2((PATH)_2]Br_2 \cdot MeOH$ (**2**)

Ni(1)−S(1)	2.166(1)	C(1)−C(2)	1.381(7)
Ni(1)−N(1)	1.920(4)	C(2)−C(3)	1.403(7)
Ni(1)−N(2)	1.983(3)	C(3)−C(4)	1.379(7)
Ni(1)−S(1A)	2.191(1)	C(4)−C(5)	1.395(6)
S(1)−C(10)	1.873(4)	C(5)−C(6)	1.500(6)
N(1)−C(1)	1.358(5)	C(6)−C(7)	1.532(6)
N(1)−C(5)	1.362(5)	C(9)−C(10)	1.528(6)
N(2)−C(8)	1.499(5)	C(10)−C(11)	1.526(5)
N(2)−C(9)	1.521(5)	C(10)−C(12)	1.533(6)
N(2)−C(7)	1.525(5)		
N(1)−Ni(1)−N(2)	91.41(14)	N(2)−Ni(1)−S(1A)	170.34(11)
N(1)−Ni(1)−S(1)	175.80(10)	S(1)−Ni(1)−S(1A)	80.98(4)
N(2)−Ni(1)−S(1)	89.62(10)	Ni(1)−S(1)−Ni(1A)	89.38(4)
N(1)−Ni(1)−S(1A)	98.12(10)		

Table 4. Selected Bond Distances (Å) and Angles (deg) for $Fe^{II}_2((PATH)_2Cl_2$ (**3**)

Fe(1)−N(1)	2.236(5)	C(17)−C(18)	1.486(7)
Fe(1)−N(2)	2.209(4)	N(2)−C(8)	1.477(8)
Fe(1)−S(1)	2.3931(18)	N(2)−C(9)	1.481(7)
Fe(1)−S(2)	2.4481(17)	N(2)−C(7)	1.492(6)
Fe(1)−Cl(1)	2.2943(17)	C(16)−C(15)	1.356(8)
Fe(2)−N(3)	2.096(5)	N(3)−C(13)	1.343(7)
Fe(2)−N(4)	2.378(5)	N(1)−C(1)	1.321(7)
Fe(2)−S(1)	2.5863(18)	N(1)−C(5)	1.340(6)
Fe(2)−S(2)	2.3484(17)	C(21)−C(22)	1.495(9)
Fe(2)−Cl(2)	2.2783(14)	C(23)−C(22)	1.522(9)
S(1)−C(10)	1.819(5)	C(22)−C(24)	1.528(7)
S(2)−C(22)	1.845(5)	C(13)−C(14)	1.371(8)
C(10)−C(11)	1.503(9)	C(14)−C(15)	1.381(8)
C(10)−C(12)	1.532(8)	C(5)−C(4)	1.380(8)
C(10)−C(9)	1.535(7)	C(5)−C(6)	1.482(8)
N(4)−C(19)	1.470(9)	C(1)−C(2)	1.378(8)
N(4)−C(21)	1.477(8)	C(6)−C(7)	1.520(8)
N(4)−C(20)	1.479(7)	C(19)−C(18)	1.530(8)
C(17)−N(3)	1.322(7)	C(2)−C(3)	1.378(9)
C(17)−C(16)	1.405(7)	C(4)−C(3)	1.371(9)
N(2)−Fe(1)−N(1)	85.92(16)	N(3)−Fe(2)−S(2)	127.68(12)
N(2)−Fe(1)−Cl(1)	111.30(12)	Cl(2)−Fe(2)−S(2)	129.92(6)
N(1)−Fe(1)−Cl(1)	91.41(14)	N(3)−Fe(2)−N(4)	88.28(19)
N(2)−Fe(1)−S(1)	84.39(12)	Cl(2)−Fe(2)−N(4)	97.80(12)
N(1)−Fe(1)−S(1)	161.15(13)	S(2)−Fe(2)−N(4)	82.39(14)
Cl(1)−Fe(1)−S(1)	107.18(6)	N(3)−Fe(2)−N(4)	93.79(14)
N(2)−Fe(1)−S(2)	134.96(12)	Cl(2)−Fe(2)−S(1)	104.78(6)
N(1)−Fe(1)−S(2)	96.06(14)	S(2)−Fe(2)−S(1)	77.69(5)
Cl(1)−Fe(1)−S(2)	113.62(6)	N(4)−Fe(2)−S(1)	156.30(13)
S(1)−Fe(1)−S(2)	79.64(6)	Fe(1)−S(1)−Fe(2)	86.31(5)
N(3)−Fe(2)−Cl(2)	102.30(13)	Fe(2)−S(2)−Fe(1)	90.55(6)

expected tridentate mode, and the five-coordinate environments around each iron atom are completed by a bridging sulfur atom from a neighboring $(PATH)Fe^{II}$ unit and a terminal chloride ligand. The dimer is neutral in charge, and there are no solvent molecules in the lattice. Each iron exhibits a geometry that is difficult to characterize as either trigonal bipyramidal or square pyramidal; analysis of the bond angles using the τ parameter[49] gives identical τ values of 0.44 for both iron centers. This τ value is close to 0.5, which indicates a structure directly between square pyramidal and trigonal bipyramidal. The most striking feature of the structure of **3** comes from the asymmetry in the Fe−S and Fe−N bond lengths. For the Fe_2S_2 core, the two chelating Fe−S bond lengths (Fe(1)−S(1) and Fe(2)−S(2)) are similar, but the bridging distances (Fe(1)−S(2) and Fe(2)−S(1)) differ from each other by 0.14 Å. The Fe(2)−S(1) distance is particularly long at 2.5863(18) Å and may be a consequence of occupying a pseudotrans position opposite N(4), since the largest angle in the Fe(2) coordination sphere is the N(4)−Fe(2)−S(1) angle. For comparison, the other $Fe^{II}_2S_2$ dimers $[(bme\text{-}daco)Fe]_2$ and $[(bme^*\text{-}daco)Fe]_2$ exhibit geometries more clearly square pyramidal and exhibit bond distances in the range 2.312(3)−2.444(4) Å.[50] Large differences in the Fe−N bonds are also observed; the Fe(1)−N(pyridine) distance is 0.14 Å longer than the Fe(2)−N(pyridine) distance, and the Fe(1)−N(amine) distance is 0.165 Å shorter than the analogous Fe(2)−N bond length. The metal−metal distance in **3** is 3.41 Å, longer than the Fe−Fe distance in $[(bme^*\text{-}daco)Fe]_2$ (3.31 Å) and clearly too long for an Fe−Fe bond.

To our knowledge, such asymmetry in the metrical parameters of a dinuclear complex with the same ligand set on each metal is rare. Given that there are no obvious steric requirements of PATH to account for the unsymmetrical structure of **3**, the asymmetry is likely a consequence of the inherent geometric preferences of the iron centers in **3**. In this regard, one conclusion is that the Fe(II) ions in **3** have a strong preference for a five-coordinate environment.

Relevance to Peptide Deformylase. The mechanism of the deformylation reaction catalyzed by PDF is currently under debate. One aspect that remains unexplained is the intriguing metal dependence of the catalytic efficiency, which drops by at least 2 orders of magnitude upon substitution of Zn(II) for Fe(II), except in PDF1A, which is isolated from the higher plant *Arabidopsis thaliana*.[10] It is especially interesting that the Zn(II) form is the least reactive, given that the zinc(II) ion is typically the native metal ion in other metallohydrolases such as carboxypeptidases as well as in the lyase carbonic anhydrase.[1,2] Our earlier work on the hydrolysis of 4-NA by **1** did not provide a good rationale for the low reactivity of Zn−PDF. In another study we suggested that the product release step involving the formate anion may be responsible for the low reactivity of Zn−PDF, based on a structural analysis of the model complex (PATH)-Zn(formate).[51] This formate complex exhibits an anisobidentate bonding mode for the formate ligand, which, in comparison to a purely monodentate bonding mode, may retard the displacement of formate by water in the final step of the enzyme mechanism. Our hypothesis was that the iron(II) form of PDF would exhibit a monodentate bonding mode for formate, while the zinc(II) form would exhibit a bidentate bonding mode.

Interestingly, recent X-ray structures from Chan and coworkers of Zn−PDF and Fe(II)−PDF with formate bound

(45) Grapperhaus, C. A.; Bellefeuille, J. A.; Reibenspies, J. H.; Darensbourg, M. Y. *Inorg. Chem.* **1999**, *38*, 3698−3703.
(46) Colpas, G. J.; Kumar, M.; Day, R. O.; Maroney, M. J. *Inorg. Chem.* **1990**, *29*, 4779−4788.
(47) Fackler, J. P. *Prog. Inorg. Chem.* **1976**, *21*, 55.
(48) Grapperhaus, C. A.; Darensbourg, M. Y. *Acc. Chem. Res.* **1998**, *31*, 451−459.
(49) Addison, A. W.; Rao, T. N.; Reedjik, J.; van Rijn, J.; Verschoor, G. C. *J. Chem. Soc., Dalton Trans.* **1984**, 1349−1456.
(50) Musie, G.; Lai, C. H.; Reibenspies, J. H.; Sumner, L. W.; Darensbourg, M. Y. *Inorg. Chem.* **1998**, *37*, 4086−4093.
(51) Chang, S.; Sommer, R. D.; Rheingold, A. L.; Goldberg, D. P. *Chem. Commun.* **2001**, 2396−2397.

to the metal center have revealed a structural trend opposite to our expectation; Fe(II)−PDF exhibits a tight, bidentate bonding mode, while Zn(II)−PDF contains a monodentate-bound formate ligand.[52] On the basis of these findings, a hybrid mechanism was proposed for Fe(II)−PDF, where the formyl oxygen atom coordinates and ultimately remains bound to the iron(II) center in the bidentate formate product, while for Zn−PDF binding of the substrate should not occur. It was suggested that the lack of substrate coordination in Zn−PDF might come from a preference of zinc to remain in a tetrahedral geometry throughout the catalytic cycle. A similar argument was previously put forth by Becker and co-workers, who suggested that tighter binding of Zn(II) by the His_2Cys donors hindered attainment of the 5-coordinate transition state necessary for a hybrid mechanism.[6]

Our findings regarding the hydrolysis of TNP and 4-NA by (PATH)ZnOH suggest an alternative explanation for the differences between Zn−PDF and Fe(II)−PDF. Our kinetic data for the reaction between the PATH−zinc complex and TNP clearly supports a hybrid mechanism, whereas a simple nucleophilic attack mechanism is inferred for the hydrolysis of 4-NA. Underlying differences in these substrates must be responsible for the change in mechanism. There may be an inherent preference for TNP to coordinate to the zinc center as compared to 4-NA. Alternatively, the phosphorus atom in TNP should be better able to accommodate the geometric strain associated with the 4-centered transition state expected from a hybrid mechanism than the carbon atom of 4-NA.[34] Thus, weak binding of 4-NA to the (PATH)−zinc complex may in fact occur, but the formation of a 4-centered transition state is unfavorable. Even though the origin of the difference in reactivity of 4-NA and TNP is not known, taken together these results point to the *flexibility* of a zinc ion in an N_2S(thiolate) environment. The existence of 4-, 5-, and 6-coordinate zinc complexes and enzymes where the zinc ion is in a ligand environment other than N_2S also shows that the zinc ion is quite flexible, exhibiting no strong preference for 4- or 5-coordination.[2] Theoretical calculations regarding zinc−water species point to the same indifference toward coordination number.[53] Given this precedent and our current experimental findings, we propose that *it is not a preference by zinc(II) for four-coordination but rather a geometric preference of iron(II) for five-coordination that causes the higher reactivity of Fe(II)−PDF compared to Zn−PDF*. Stated another way, there is no significant energetic penalty for the Zn(II) center to bind the formyl group, but there is an energetic gain for the Fe(II) center to bind the formyl group during the hydrolysis reaction, thereby favoring a hybrid mechanism. This reasoning also allows for the possibility of active Zn−PDFs in certain cases, such as PDF1A from *A. thaliana*.[10] The formate groups in bacterial (formate)Zn−PDF and (formate)Fe^{II}−PDF are also stabilized by hydrogen bonds to the backbone NH group of Leu91 and the side chain of Gln50,[52] indicating that the formyl carbonyl oxygen prior to hydrolysis may also be H-bonded to these groups. These H-bond interactions can further discourage substrate coordination in Zn−PDF.

Implicit in the former explanation is the assumption that a bidentate bonding mode for (formate)Fe^{II}−PDF does not cause a product inhibition effect. This assumption is correct if substitution by H_2O of both the bidentate $(O_2CH)Fe^{II}$−PDF and monodentate (O_2CH)Zn−PDF intermediates is rapid and therefore not part of the rate-determining step or if the formate species undergoes facile interconversion between bidentate and monodentate modes. The latter transformation would not be observable in the static crystal structures of the enzyme.

Summary and Conclusions

The kinetic studies on the hydrolysis of TNP promoted by (PATH)ZnOH point to a hybrid mechanism. This mechanism accounts for the significant rate acceleration, pH−rate dependence, and activation parameters that are observed, and it suggests that the zinc coordination sphere is flexible enough to accommodate the binding of a phosphate ester. These findings are different from those for the hydrolysis of the related carboxylic ester 4-NA, which showed 4-NA reacted through a simple nucleophilic attack mechanism. Interestingly, new information on PDF from X-ray structures of bacterial (formate)Fe^{II}−PDF and (formate)Zn−PDF suggest that the difference in reactivity between Fe^{II}−PDF and Zn−PDF may be due to the presence or absence of a hybrid mechanism during the hydrolysis of the formyl substrate. Our results show that a zinc ion in a PDF-type environment, i.e., an N_2S(thiolate) donor set, is flexible and can exhibit both simple nucleophilic attack and hybrid mechanisms of hydrolysis depending upon the substrate. These findings indicate that the different reactivities of Zn− and Fe(II)−PDF may arise from the iron(II) center's strong preference for a five-coordinate geometry, thereby ensuring a hybrid mechanism, while the analogous zinc(II) center does not exhibit this preference and operates through a less efficient nucleophilic attack mechanism. Structural characterization of $(PATH)_2Fe_2Cl_2$ supports the notion that iron(II) prefers a five-coordinate environment in the presence of N,S-type donor ligands. Recent results on the structural analysis of an iron(II)−formate complex combined with theoretical calculations comparing zinc(II)− and iron(II)−formate model complexes support these conclusions and will be reported in due course.[54]

Acknowledgment. The National Institutes of Health (Grant GM62309 to D.P.G.) are gratefully acknowledged for support of this work. D.P.G. also thanks the Alfred P. Sloan, Jr., Foundation for an Alfred P. Sloan, Jr., Research Fellowship.

Supporting Information Available: X-ray crystallographic files in CIF format for **2** and **3**. This material is available free of charge via the Internet at http://pubs.acs.org.

IC0511571

(52) Jain, R.; Hao, B.; Liu, R.; Chan, M. K. *J. Am. Chem. Soc.* **2005**, *127*, 4558−4559.
(53) Bock, C. W.; Katz, A. K.; Glusker, J. P. *J. Am. Chem. Soc.* **1995**, *117*, 3754−3763.
(54) Karambelkar, V. V.; Zhang, Y.; Zhao, C.; Goldberg, D. P. Submitted for publication.